Sigma J Eng Nat Sci, Vol. 44, No. 4, pp. 2347−2363, August, 2026

Sigma Journal of Engineering and Natural Sciences
Web page info: https://sigma.yildiz.edu.tr
DOI: 10.14744/sigma.2026.2100

Research Article

Estimating above ground biomass in black pine forest using ALOS-1 data and machine learning methods

Şükrü Teoman GÜNER[1], Omer Gokberk NARIN[2,*], Aydın ÇÖMEZ[3], Eren Gürsoy ÖZDEMİR[4], Caglar BAYIK[5], Saygın ABDIKAN[6]

[1]*Department of Forestry, Bartın University, Bartın, 74100, Türkiye*
[2]*Department of Geomatics Engineering, Afyon Kocatepe University, Afyonkarahisar, 03200, Türkiye*
[3]*General Directorate of Forestry, Aegean Forestry Research Institute, Urla, İzmir, 35661, Türkiye*
[4]*Department of Architecture and Urban Planning, Bartın University, Bartın, 74100, Türkiye*
[5]*Department of Geomatics Engineering, Zonguldak Bulent Ecevit University, Zonguldak, 67100, Türkiye*
[6]*Department of Geomatics Engineering, Hacettepe University, Ankara, 06800, Türkiye*

ARTICLE INFO

Article history
Received: 08 September 2024
Revised: 15 January 2025
Accepted: 19 February 2025

Keywords:
Aboveground Biomass; ALOS PALSAR; Machine Learning; Pinus Nigra

ABSTRACT

Within the sustainable development goal 'climate action framework,' forests play a vital role in enhancing climate resilience. The data obtained from these ecosystems are expected to significantly contribute to shaping regional forestry policies and advancing climate-related studies. Above-ground biomass (AGB) is a substantial parameter of the ecosystem cycle and is used to estimate forest carbon storage. Knowledge of the spatial distribution of AGB supports the management of forests and understanding of climate change's effects. This study aims to analyze the relationship and to estimate biomass using machine learning methods between the AGB of a black pine (*Pinus nigra*) plantation forest obtained from ground measurements and the global mosaic L-band ALOS-PALSAR Synthetic Aperture Radar (SAR) image. The forest is distributed in western Inner Anatolia to the Black Sea, Marmara, and inner Aegean regions of Türkiye. Fieldwork was carried out in 44 plots distributed across different locations in Türkiye. The mean diameter, mean height, stand age, stand stock, stocking density, and basal area were determined for each sample. The aboveground tree masses of the sample trees were calculated. The relationship between ground-based AGB calculation and remote sensing ALOS data was obtained. This study estimated the AGB using linear regression, Random Forest, XGBoost, and Convolutional Neural Network (CNN) techniques. In addition to backscatter images of dual polarimetric (HH and HV) data, we created Normalized Difference Polarization Index (NDPI) and Co-polarized Ratio (CPR) images. Twelve scenarios were created using these four variables of ALOS data and their AGB estimation results were compared. . The highest AGB estimation performance obtained with the CNN model was achieved by combining HV polarization and CPR features, resulting in an R^2 value of 0.448 and an RMSE of 59.726 t/ha. The findings indicate that HV polarimetric data and integrating additional features further improved estimation capability. Overall, the findings demonstrate that integrating SAR imagery with CNN-based approaches provides an efficient, economically viable framework for multi-temporal forest biomass estimation. Such an approach has considerable potential to support large-scale forest carbon monitoring, sustainable forest management practices, and climate change mitigation policies at both national and global scales, including in Türkiye.

Cite this article as: Güner ŞT, Narin ÖG, Çömez A, Özdemir EG, Bayık Ç, Abdikan S. Estimating above ground biomass in black pine forest using ALOS-1 data and machine learning methods. Sigma J Eng Nat Sci 2026;44(4):2347−2363.

***Corresponding author.**
*E-mail address: gokberknarin@aku.edu.tr

This paper was recommended for publication in revised form by Editor-in-Chief Ahmet Selim Dalkilic

Published by Yıldız Technical University Press, İstanbul, Turkey

INTRODUCTION

The use of fossil fuels in human activities and the reduction of forests lead to an increase in carbon dioxide in the atmosphere. The increase in carbon dioxide concentration in the atmosphere is seen as the main cause of global climate change [1]. Forest ecosystems, which have the largest carbon pool among terrestrial ecosystems, have an important place in the global carbon cycle owing to their biomass production by binding carbon dioxide in the atmosphere to their bodies through photosynthesis [2]. Forests store more than 80% of the carbon stock in terrestrial ecosystems [3]. The determination of the produced biomass can make important contributions to a better understanding of the carbon cycle and thus to the determination of adaptation strategies to climate change. Conventional methods use biomass on inventory data with allometric equations or expansion factors of forest biomass [4, 5]. Terrestrial-based measurement techniques are mostly used in the determination of tree biomass in forest ecosystems [6]. However, these techniques have some limitations. Terrestrial techniques include tree species-specific biomass equations or tree trunk volume data based on forest inventory. In order to use the biomass equations, it is necessary to determine the diameters and heights of the trees by ground measurements. In the forest inventory in Türkiye, the diameter and height values of trees and the volumes of the stem with bark are determined in 10-year periods. Biomass can also be calculated using the biomass conversion and expansion factors from the tree stem volume data obtained. However, the calculated biomass belongs to different years and cannot reflect the current situation. Therefore, biomass determination methods that require less time and labor are needed.

Biomass estimation using satellite images and image processing techniques is used as a much faster and more economical method for large areas. Remote sensing data through passive (optical) and active sources such as Synthetic Aperture Radar (SAR) and Light Detection and Ranging (LiDAR) are efficient tools to estimate the structure and composition of the forest ecosystem as well as the forest Aboveground biomass (AGB) [7-10]. Estimating AGB by optical techniques that determine the correlation between the spectral response and the ground data obtained from the field plots is effective for the estimation of foliar biomass components. However, it does not penetrate the woody biomass, dense forest canopy, and saturate at low biomass amounts and has limitations due to atmospheric conditions [11, 12]. Compared to optical sensors, SAR sensors are more effective because they can acquire data in cloudy conditions and day and night. Among the SAR systems L-band ALOS data has been preferred due to its longer wavelength that can penetrate through the forest cover [13]. Previous studies showed its potential over different forest types. Englhart et al. [14] studied AGB estimation in tropical forests, in Kalimantan, Indonesia, using TerraSAR – X (X band) and Advanced Land Observing Satellite (ALOS) Phased Array L-band Synthetic Aperture Radar (PALSAR) sensor (L band) SAR data. They concluded that ALOS PALSAR backscatter was more sensitive to AGB than TerraSAR– X. George-Chacon et al. [15] achieved the best fit using machine learning when Sentinel-2 and ALOS PALSAR were combined for the semideciduous tropical forest of Mexico. The linear regression (LR) method was the most widely used parametric method for AGB estimation in previous studies [16]. Non-parametric techniques including machine learning methods and deep learning methods have been used for forestry research such as canopy height [17] and AGB estimation [18, 19]. Convolutional neural networks (CNNs) are widely applied for image classification and change detection studies [20-22] and are rarely used for forest AGB estimation [19]. In the case of pixel-based analysis, one-dimensional CNN (1D-CNN) is considered for parameter estimation studies [23].

Black pine (*Pinus nigra* Arn.) is widespread in Southern Europe, Northwest Africa, and Türkiye (in Anatolia) [24]. There are five subspecies systematically, ssp. nigra, ssp. salzmannii, ssp. laricio, ssp. dalmatica and ssp. pallasiana [25]. Among these subspecies, Anatolian black pine (*Pinus nigra* J. F. Arnold. subsp. *pallasina* (Lamb.) Holmboe var. *pallasiana*) [26] naturally distributed in Türkiye, Thrace, Crimea, Balkans, Southern Carpathians, Cyprus, Western Caucasus, and Western Spread in Syria [27, 28]. Black pine (*Pinus nigra* subsp. *pallasina* (Lamb.) Holmboe) in pure form or mixed with species such as oak, fir, pine, and juniper in Türkiye at 165-2150 meters; it spreads over an area of 4.5 million hectares in Marmara, Black Sea, Aegean, Mediterranean, and Central Anatolia Regions and constitutes 18.3% of the forest areas [29, 30]. Black pine has been one of the most widely used species in afforestation studies due to its ability to grow on poor soils as well as its resistance to both arid and cold conditions [31]. The several equations were developed toestimate the biomass of black pine in previous studies [32, 33]. Balenovic et al. [34], on the other hand, explained the biomass of the black pine species using high-resolution aerial stereo-images with the independent variables of the crown and tree height they estimated. However, Balenovic et al. [34] used remote sensing data to estimate the independent variables in the biomass equations. Günlü et al. [35] estimated the AGB of pure black pine forest using high resolution WorldView-2 optical data. Turgut and Günlü [36] detected the aboveground biomass of *Pinus nigra* with 32.78 t/ha Root Mean Square Error (RMSE) and 0.55 coefficient of determination (R^2) using Landsat 8 OLI satellite image and multiple linear regression. Bulut et al. [37] predicted AGB of coniferous, broadleaf, and mixed stands using Sentinel-2 optical data. Vatandaslar and Abdikan [38] estimated carbon stock using ALOS-2 data and forest inventory for a black pine and mixed forest (Lebanese cedar, Taurus fir, and juniper). Total carbon stock is estimated at R^2 of 0.78 with HH of ALOS-2 data. Bulut [39] studied AGB prediction of pure Calabrian pine (*Pinus brutia* Ten.) in Türkiye. The study used multiple regression analysis (MLR) and support vector machines (SVM) with Landsat-8 data. The SVM provided higher R^2 for validation data than MLR. Li et al. [40] estimated AGB using Landsat-8 and Sentinel-1A data with linear Regression, XGBoost, and Random Forest (RF) methods in subtropical forests in China's Hunan province. As a result of the study, they stated that the XGBoost algorithm gave better results than other methods. They obtained results of R^2=0.38 in estimation with Sentinel-1A, R^2=0.66 in estimation with Landsat-8, and R^2=0.75 in the combined use of Sentinel-1A and Landsat-8. Although several studies have been conducted on the estimation of the biomass of some pine species by remote sensing [12, 36, 38, 39], there is no research on pure *Pinus nigra* forest with SAR data in Türkiye. Meanwhile, considering the other biomass studies, the literature on biomass studies of semi-arid region forests is limited [41].

This study investigates the relationship between biomass data collected from various regions in Türkiye for pure *Pinus nigra* forests and global ALOS-PALSAR satellite data, given the unavailability of suitable optical data. While CNN-based approaches for AGB estimation are relatively limited, this study also addresses the comparative performance of CNN with other widely discussed methods in the literature, such as RF and XGBoost. The CNN model was selected to estimate AGB using ground-truth measurements from 44 plots in a pure *Pinus nigra* forest in Türkiye. The CNN model was compared with RF, XGBoost, and linear regression to evaluate its performance. The model was trained using dual-polarimetric backscatter images (HH and HV) together with two additional indices derived from ALOS-PALSAR mosaic data: the Normalized Difference Polarization Index (NDPI) and the Co-polarized Ratio (CPR). These variables provided complementary information and improved the representation of forest structure. A CNN was used because it can automatically learn relevant patterns directly from the input data, minimizing the reliance on manual feature extraction. It can offer advantages over traditional machine learning methods, which rely on manually selected features. This capability allows CNNs to capture complex spatial patterns embedded in remote sensing data. Because CNNs can effectively handle complex spatial data and have been successfully applied in similar environmental studies, they are well suited for AGB estimation in forest ecosystems. Accurate forest biomass prediction contributes to monitoring carbon stocks, assessing emissions reductions, and informing sustainable forest management strategies. Thus, cost-effective carbon inventory methods are needed for climate change policies.

MATERIALS AND METHODS

Study Area

The research was completed in wide area located between the latitudes of 38°23′00″ - 41°30′58″N and longitudes of 29°33′33″ - 30°03′37″ E on a transition zone. It continued from Marmara, Inner Aegean regions to Western Inner Anatolia and the Black Sea, of Türkiye (Figure 1). The common bedrocks in the study area include dacite, rhyolite, basalt, andesite, granite, volcanic tuff, agglomerate, breccia, quartzite, mica schist, calcareous, and serpentine [42]. The most common soil types are cambisols and luvisols, according to IUSS Working Group WRB [43]. Climatic data were derived from the nearest meteorological stations. Mean annual temperatures vary from 8.9 °C to 14.4 °C while annual precipitation ranges from 374 mm to 796 mm [44]. The climate type of the study area was classified

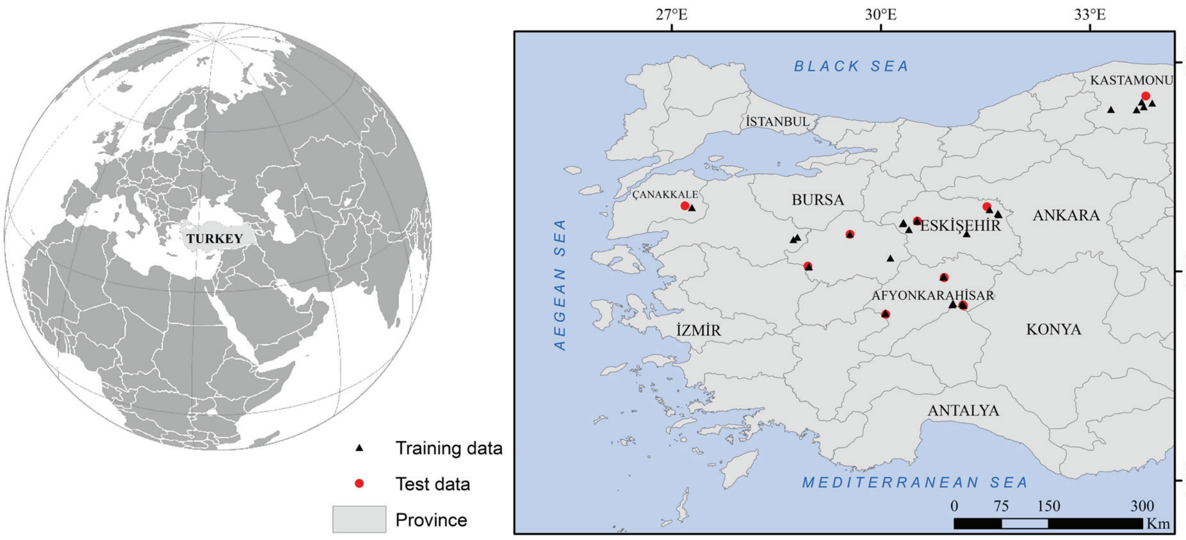

Figure 1. Location of the study area.

as semi-arid to humid using the Erinç method [45]. The elevation of the study sites ranged from 417 m to 1587 m.

Experimental Design and Sampling Procedure

Sample plots were chosen from a total of 44 areas differing in elevation, aspect, sloping degree, slope position and stand development stage [SDF=small diameter forest (dbh<8.0 cm), MDF=medium diameter forest (dbh=8.0-19.9 cm), LDF=large diameter forest (dbh=20.0-35.9 cm)]. Some characteristics of the stands in the research areas are given in Table 1 [46]. The fieldwork were conducted between 2010 and 2012.

Sample plots were taken in the form of square or rectangular (10×10, 10×20, or 20×20 m) and large enough to contain at least 15 individual trees. A healthy individual tree, with no crown and branch damages, and under pressure, was cut. The diameter and height of all individuals were measured in the sample plots. Tree height was measured by a tape measure with cm precision, after cutting down the tree, and the age was determined by counting the annual rings on the stump (Figure 2). After the branches of the cut tree had been trimmed, the trunk was divided into 2 m sections. Then, the fresh weight of the 2-meter-long trunk sections was measured with a scale. To convert the fresh weights of the trunk into dry weight, 5 cm thick discs were taken from the middle of each section to determine their moisture content. The needles were separated from the branches and weighed separately. In order to determine

Table 1. Stand parameters of the sample plots (Mean±SE)

Stand properties	Development stage		
	SDF	MDF	LDF
Number of sample plots	14	12	18
Mean diameter (dbh,cm)	4.9±0.8	16.5±0.9	25.4±0.9
Mean height (m)	2.38±0.25	8.88±0.59	14.15±0.69
Stand age (year)	10.8±1.1	37.0±2.4	45.1±1.8
Standing stock (m^3/ha)	6.988±2.912	173.202±21.643	303.572±32.800
Stocking density (tree/ha)	2510±267	1546±146	866±132
Basal area (m^2/ha)	6.43±1.75	33.15±3.07	41.51±4.21

SE: standard error, SDF: small-diameter forest (dbh < 8.0 cm), MDF: medium-diameter forest (dbh=8.0-19.9 cm), LDF: large-diameter forest (dbh=20.0-35.9 cm)

Figure 2. Fieldwork photos of the study area in Eskişehir Province.

oven-dry weights in the laboratory, sub-samples were taken from the stem (5 cm thick discs), branches (dry and live), and needles, and their fresh weights were determined in the field [46].

Above Ground Mass Calculation

Sub-samples taken from the field were oven-dried at 65 °C to a constant weight [33] and then weighed again to calculate the moisture correction factor for the dry weight of the tree biomass to calculate the amount of bark, the ratio of the disk weight without bark to that of with bark was multiplied by the trunk biomass. Then, the above-ground tree masses of the sample trees were calculated by adding the dry weight of needles, dead and live branches, bark-free trunk, and bark.

Data Analysis

Diameter at breast height (dbh), height (h), and dbh^2h index were used as independent variables to estimate the above-ground tree mass (kg/tree) of a single tree. As a result of regression analysis, the equation with the smallest standard error and the highest Coefficient of determination (R^2) was obtained with the compound function (Equation 1). Then, using this equation, the above-ground tree masses in the sample areas were calculated and these values were converted to hectares (t/ha).

$$B_{ABOVEGROUND} = axb^{dbh} \tag{1}$$

where B: tree mass (kg/tree), a and b equation coefficients, dbh: diameter at breast height.

Remote Sensing Data

In this study, the mosaic ALOS PALSAR data for the year 2009 is used for the analysis. It was the mission of the Japanese Aerospace Exploration Agency (JAXA). Its 25 m spatial resolution mosaic data is open to the public [47]. The data is distributed in two polarizations horizontal transmitted and horizontal received (HH) and horizontal transmitted vertical received (HV). The pre-processing steps and geometric and radiometric corrections of L-band data have been applied by JAXA [47]. In the case of geometric correction, SRTM3 data was used. The amplitude backscatter values were converted to gamma nought [48,49] using the equation below;

$$\gamma° = 10 \text{ x } \log_{10}(DN^2) + CF \tag{2}$$

Where $\gamma°$ is the backscatter coefficient, DN and the CF are the digital number of amplitude data and the calibration factor which is -83 dB, respectively. Two arithmetic equations were also used to derive additional variables. These are the Normalized Difference Polarization Index (Υ_{HH} - Υ_{HV}) / (Υ_{HH} + Υ_{HV}) and Co-polarized Ratio (CPR) (Υ_{HV} / Υ_{HH}). In addition to these 4 data, 8 data sets were created and a total of 12 scenarios were evaluated (Table 2). An example of a visual interpretation of the SAR data is shown in Figure 3. The HH and HV values are represented in decibels (dB) and range between 10.3 dB and -36.6 dB. The location of the pine forest appears brighter in SAR data.

Convolutional Neural Network

A one-dimensional Convolutional Neural Network (1D-CNN) architecture was employed for Above-Ground Biomass (AGB) estimation. This architecture utilized a one-dimensional convolutional filter as the input layer and comprised a convolutional layer, a flattening layer, dense layers, and an output layer. For this study, the selected hyperparameters included 16 filters, the ReLU activation function, and 250 training epochs. A trial and error method was used to select these parameters. The Adam optimization algorithm was utilized to optimize the model parameters, as recommended in prior research [50]. RMSE was used as the loss function and the test/loss graph of the best scenario was given in Appendix-1. In the analysis randomly, 33 data were used for training the model and 11 data were used for the test.

Extreme Gradient Boosting

Extreme gradient boosting (XGBoost) is a highly efficient ensemble learning algorithm commonly applied to classification and regression tasks, particularly in structured data contexts. Known for its robustness when handling large datasets and complex models, XGBoost constructs a strong predictive model by iteratively combining weak learners and addressing the errors of preceding models at each step. XGBoost builds on the gradient boosting framework, by introducing several features to enhance computational efficiency, performance, and predictive accuracy [51]. In our study, the R programming language and the

Table 2. The scenarios and the variables used for the analysis

Scenarios	Variables	Scenarios	Variables
S1	Υ_{HH}	S7	Υ_{HH}, Υ_{CPR}
S2	Υ_{HV}	S8	Υ_{HV}, Υ_{NDPI}
S3	Υ_{NDPI}	S9	Υ_{HV}, Υ_{CPR}
S4	Υ_{CPR}	S10	Υ_{HH}, Υ_{NDPI}, Υ_{CPR}
S5	Υ_{HH}, Υ_{HV}	S11	Υ_{HV}, Υ_{NDPI}, Υ_{CPR}
S6	Υ_{HH}, Υ_{NDPI}	S12	Υ_{HH}, Υ_{HV}, Υ_{NDPI}, Υ_{CPR}

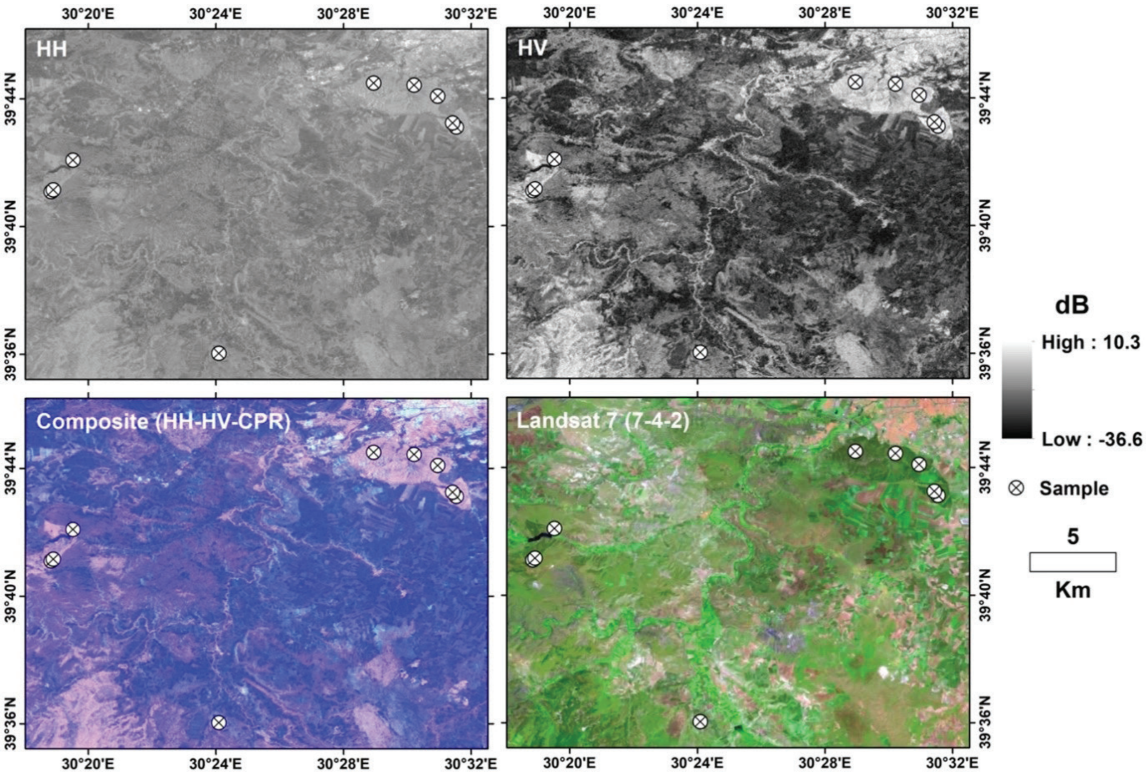

Figure 3. An example of a SAR image over Eskisehir is located in Figure 1. In the upper row, examples of ALOS HH and HV polarimetric data are given, in the lower row, RGB data created from HH-HV and CPR data and Landsat 7-4-2 bands are given. Landsat data is used only for visual interpretation to show the location of the forest.

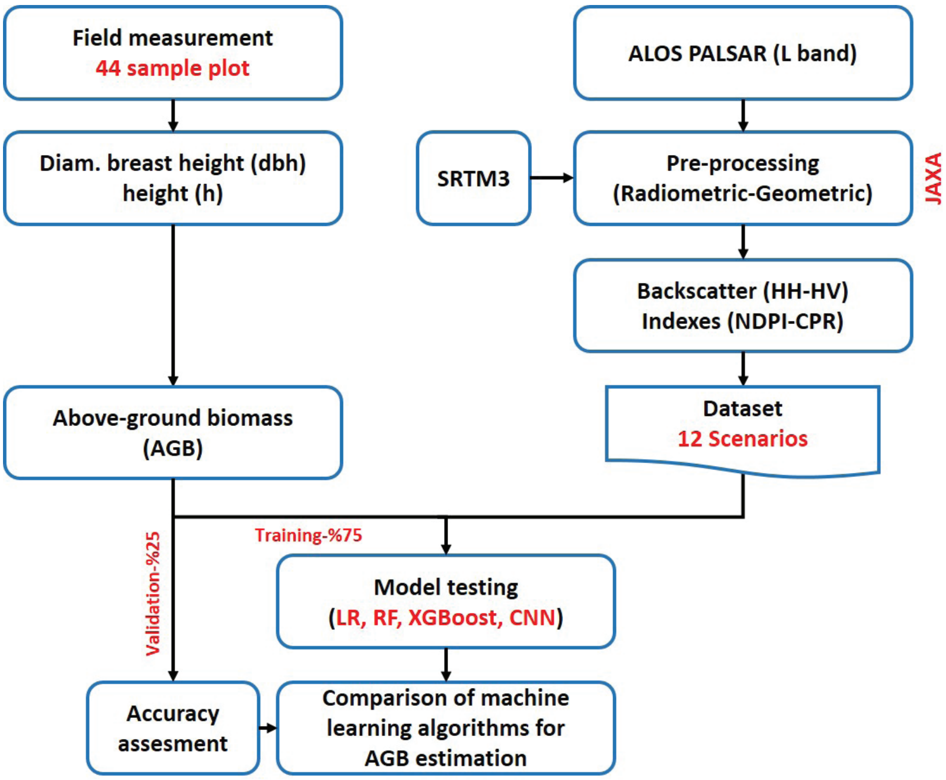

Figure 4. The graph shows the workflow used for AGB estimation.

XGBoost package were used [52]. The parameters were tuned during the model training phase. In order to make the best grid search, the values were chosen primarily based on the results of the previous studies [53].

Parameters, *nrounds* is "50, 100, 200, 250, 500", *max_depth* is "3, 5, 7", *eta* is "0.01, 0.02, 0.05", *gamma* is "0.1, 0.3, 0.5", *min_child_weight* is "1,2,3,4,5", *subsample* is "0.5, 0.6, 0.7", and *colsample_bytree* is chosen "1, 3, 5". According to these values, the best results were automatically selected in model training and the model was trained. Sample results are included in Appendix-2.

Random Forest

Random Forest is an ensemble learning method used for machine learning and statistical analysis. Random Forest improves prediction accuracy by combining multiple decision trees and is a powerful method for dealing with complex datasets. One of the advantages of Random Forest is that it is resistant to noise and overfitting in the dataset [54]. In our study, the R programming language and the Random Forest package were used [55]. Parameters were tuned during the model training phase. In order to make the best Grid search, the values were chosen primarily according to the results of [40]. Parameters *ntree* is increased from 10 to 300 in step 10 and *mtry* is increased from 1 to 10 in step 2 (Appendix-3). The workflow of our methodology for estimating AGB is given in Figure 4.

RESULTS AND DISCUSSION

Findings of the Tree Mass

The best independent variable predicting the above-ground tree mass was diameter at breast height, and the best model was obtained with the compound function (Table 3). Above-ground tree mass was found to be the lowest (10.525 t/ha) in SDF stands and the highest (166.374 t/ha) in LDF stands (Table 4).

Biomass Estimation With Machine Learning

In the analysis for each scenario, the relationship between AGB data estimated from the fieldwork and ALOS PALSAR backscatter data was evaluated. The results showed that the overall r values ranged between 0.52 and 0.72 (Figure 5). The highest correlation was obtained with HH polarized data (r=0.720) and HV polarization followed it with an r=0.632. The relationship between AGB and the indices derived from backscatter values were close to each other. However, CPR had a positive correlation (r=0.553), while NDPI gave a negative (r=-0.517). The relationship between HH and HV also showed a high value (r=0.879). Considering the relationship between the backscatter values of two polarizations and the indices, HH polarized data provided a higher value (r=-0.654 and r=0.625) than HV polarized data (r=-0.230 and r=0.236).

The estimation analysis was composed of 33 training and 11 testing data. In addition to the CNN method, LR, RF, and XGBoost were also applied for comparison (Figure 6). In general, models in S7, S8, and S9 showed successful results; however, models gave unsuccessful results in S2, S3, and S4 (Figure 6). If RMSE and R^2 are compared in detail, CNN provided higher R^2 and lower RMSE values compared to the LR, RF, and XGBoost methods. All methods showed good results in different scenarios. The CNN showed the best performance in S9 (RMSE=59.73 t/ha, R^2=0.45). LR showed the best performance after CNN in S7 (RMSE=61.57 t/ha, R^2=0.41). While the RF method gave the same R^2 results as LR, it showed slightly worse results (RMSE=65.65 t/ha, R^2=0.41). Although the XGBoost method gave better RMSE than RF, it showed the worst result in R^2 (RMSE=64.28 t/ha, R^2=0.36) (Table 5).

Table 3. Single tree regression model for above-ground biomass

Equation	R^2	Standard error	F ratio	*p*	Constants	
					a	b
$B_{aboveground} = a \times b^{\,dbh}$	0.952	0.30	873.64	0.000	4.9953^{***}	1.1560^{***}

B= biomass (kg/tree), *dbh*= diameter at breast height (cm), *h*= tree height (m), R^2= coefficient of determination, *p*: significance, ***: $p<0.001$

Table 4. Above-ground biomass according to development stage

Biomass	Development stage		
	SDF	MDF	LDF
Above-ground (t/ha)	10.525±2.657	107.093±11.289	166.374±17.353

SE: Standard error; SDF: Small-diameter forest (dbh < 8.0 cm); MDF: Medium-diameter forest (dbh=8.0-19.9 cm); LDF: Large-diameter forest (dbh=20.0-35.9 cm).

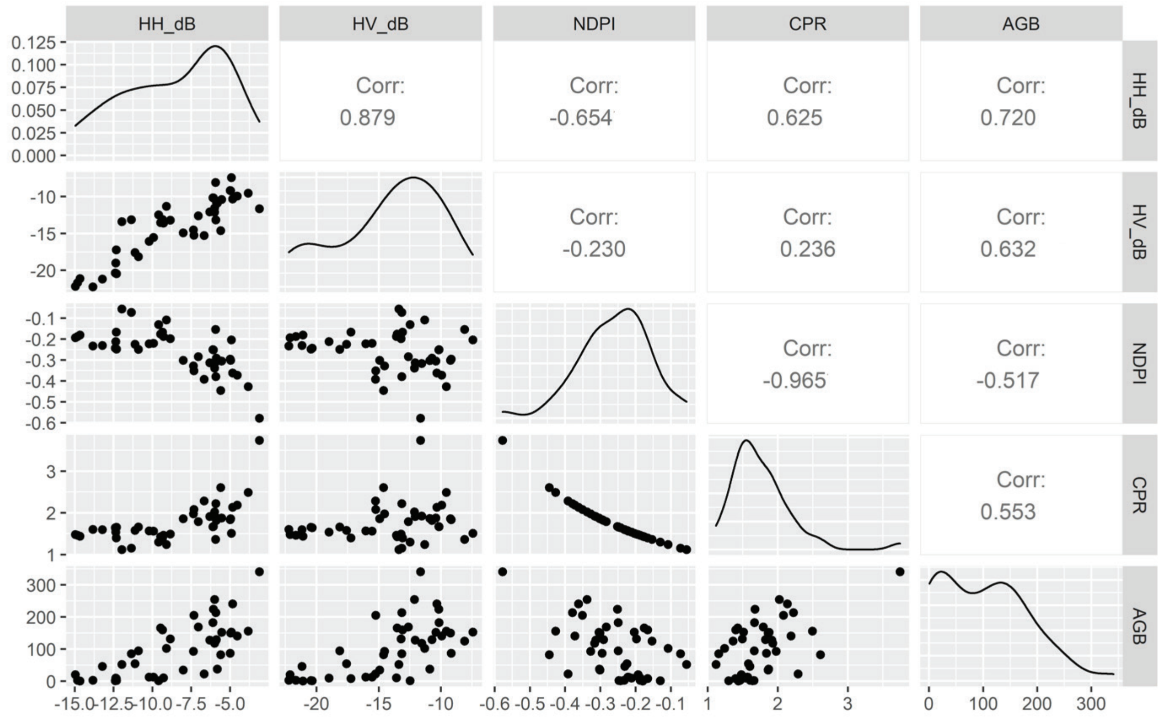

Figure 5. The correlation coefficient and scatter plot between AGB and variables derived from SAR data.

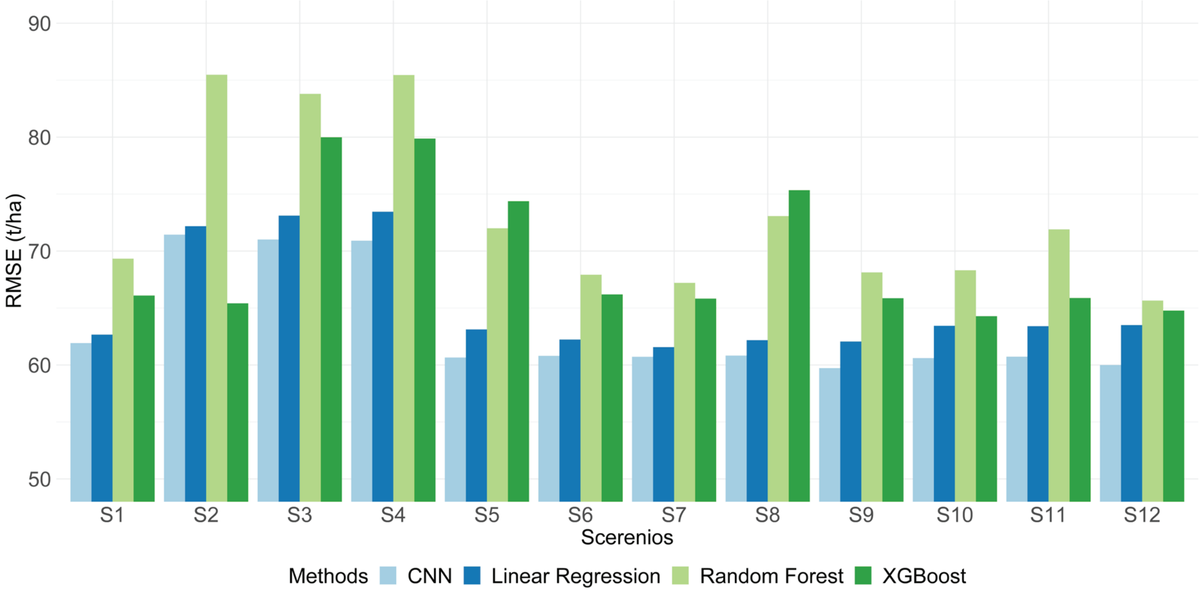

Figure 6. The comparison of CNN, LR, RF, and XGBoost with regard to RMSE.

The study was conducted using four models: CNN, RF, XGBoost, and LR. Considering the previous studies in Türkiye, estimation studies for black pine were mostly carried out with optical data [35, 36, 55]. Günlü et al. [56] used Landsat with vegetation indices and applied the Multiple Linear Regression (MLR) method. The results revealed that vegetation indices showed R^2=0.61 and RMSE=8.50 t/ha AGB using 130 samples. Günlü et al. [35] used 86 samples with high-resolution Worldview-2 bands and the texture information for the AGB estimation. The results of the

Table 5. The R^2 and RMSE values of the test data. While green color shows the best results, red values show the lowest values

Scenarios	Variables	Linear Regression		CNN		XGBoost		Random Forest	
		R^2	RMSE	R^2	RMSE	R^2	RMSE	R^2	RMSE
S1	Υ_{HH}	0.38	62.66	0.34	61.92	0.30	66.09	0.21	69.33
S2	Υ_{HV}	**0.00**	72.18	0.18	71.44	0.31	65.41	0.06	**85.47**
S3	Υ_{NDPI}	0.22	73.11	0.19	71.01	0.09	79.98	0.09	83.79
S4	Υ_{CPR}	0.24	73.45	0.24	70.91	0.11	79.87	0.09	85.45
S5	Υ_{HH}, Υ_{HV}	0.36	63.12	0.42	60.65	0.17	74.37	0.19	72.00
S6	Υ_{HH}, Υ_{NDPI}	0.39	62.23	0.42	60.80	0.32	66.19	0.32	67.92
S7	Υ_{HH}, Υ_{CPR}	0.41	61.57	0.41	60.71	0.32	65.82	0.33	67.21
S8	Υ_{HV}, Υ_{NDPI}	0.39	62.17	0.41	60.82	0.11	75.34	0.14	73.07
S9	Υ_{HV}, Υ_{CPR}	0.41	62.06	**0.45**	**59.73**	0.33	65.86	0.29	68.12
S10	Υ_{HH}, Υ_{NDPI}, Υ_{CPR}	0.38	63.44	0.42	60.61	0.36	64.28	0.28	68.31
S11	Υ_{HV}, Υ_{NDPI}, Υ_{CPR}	0.39	63.41	0.43	60.72	0.35	65.88	0.16	71.90
S12	Υ_{HH}, Υ_{HV}, Υ_{NDPI}, Υ_{CPR}	0.39	63.49	0.43	59.99	0.34	64.77	0.41	65.65

ANN method provided RMSE ranging from 69.12 to 85.35 t/ha (R^2=0.34-0.57) whereas the RMSE of MLR was 85.15 t/ha (R^2=0.34).

Bulut et al. [37] used single-date Sentinel-2 data for the AGB estimation on coniferous, broadleaf, and mixed forest types with 2185 samples in total. They used MLR and regression kriging (RK) methods on reflectance and vegetation indices separately. Considering the coniferous forest, the results of MLR provided better results (RMSE = 48.90 t/ha and 47.15 t/ha) than the results of RK (RMSE = 51.28 t/ha and 49.73 t/ha). The vegetation indices provided better results than reflectance data. Bulut [39] used Landsat-8 with machine learning approaches for the AGB prediction over Calabrian pine in Türkiye. The study showed that the SVM approach provided better results over MLR and vegetation indices contributing to achieving successful prediction.

Previous studies predominantly employed the MLR method for AGB estimation in pine forests. In contrast, this study's results show that the models (LR, CNN, XGBoost, and RF) perform differently across various scenarios with single and multiple variables. LR and CNN models showed moderate performance in scenarios (S1–S4), where single variables were used. The R^2 values ranging from 0.00 to 0.38 and RMSE values between 61.92 and 73.45. XGBoost performed better in scenarios S1 and S2, but its results were not consistent across all cases. On the other hand, RF had the weakest overall performance, with a relatively low R^2 and high RMSE. Including additional variables generally improved model performance in the bivariate scenarios (S5–S9). Scenario S9 produced the best performance for the CNN model, achieving an R^2 value of 0.45 and the lowest RMSE (59.73) than the other models. The LR model also showed relatively strong and stable results, although it consistently remained slightly below CNN in terms of accuracy. XGBoost demonstrated some improvement across several cases; however, overall it still lagged behind both CNN and LR in predictive performance. RF indicated partial improvement, particularly in scenarios S7 and S9. However, its overall performance remained below that of the alternative models. When all three variables were used together (S10–S11), CNN continued to outperform the alternatives, achieving R^2 values of 0.42-0.43 and consistently producing the lowest RMSE across all tested methods. LR maintained stable and reliable performance in these scenarios, although it still trailed slightly behind CNN in predictive accuracy. XGBoost benefited from the extra variable and reaching an R^2 of 0.36 under S10. RF improved modestly, yet its estimates continued to lag behind those of CNN and XGBoost. In the four-variable configuration (S12), CNN continued to provide the best results (R^2= 0.43; RMSE= 59.99). RF achieved its strongest performance in this senario (R^2= 0.41; RMSE= 65.65), whereas LR and XGBoost performed at comparable levels, recording R^2 values of 0.39 and 0.34 respectively, yet neither reached the accuracy of CNN. Adding more predictors generally improved model performance, particularly for XGBoost and RF; but neither matched CNN's robustness, especially in more complex situations (Table 5).

Huang et al. [57] assessed six modeling strategies LR, RF, SVR, XGBoost, LASSO regression, and an ensemble approach for blood pressure prediction during hemodialysis. Of those methods shared with the current study, XGBoost recorded the lowest test accuracy (RMSE= 17.65, R^2= 0.41), while LR (RMSE= 16.39, R^2= 0.48) and RF (RMSE= 16.24, R^2= 0.49) performed at roughly equivalent levels. Smith et al. [58] compared MLR with RF and found that MLR performed better, which is similar to our study. Dong et al. [19] studied estimation of bamboo AGB in in southern China. They used different machine learning approaches (RF, SVR, ANNs, and CNNs) with optical WorldView-2 imagery. They reported that, RF, SVR, and CNN-based methods all outperformed conventional ANNs with respect to prediction accuracy. Schäfer et al. [59] compared CNN and RF models using point cloud data from forested areas in Canada, Poland, and the Czech Republic, and found that CNN architectures produced superior results when sufficiently large training datasets were available. The findings of this study further strengthen the suitability of CNN-based architecture for AGB modelling.

The Υ_{HV} polarization data exhibited higher predictive capability than Υ_{HH} across the tested scenarios. This observation is consistent with previous studies based on ALOS datasets [60–63]. However, some studies also indicated the advantage of HH polarization over HV [13, 64, 65]. When two variables that were derived from backscatter values were compared, CPR (S4) provided a slightly higher contribution than NDPI (S3). The advantage of CPR was also evident when added to the HH and HV polarized images individually. The combination of Υ_{HV} and Υ_{CPR} (S9) achieved the best result with RMSE= 59.726 t/ha and R^2= 0.448. Li et al. [40] used Sentinel-1A SAR and with Landsat-8 optical data for AGB estimation. They compared LR, RF, and XGBoost methods. The results showed that Sentinel-1A-only results were relatively weak, with R^2 values of 0.03, 0.28, and 0.38 for LR, RF, and XGBoost, respectively. Considerin their results, the L-band ALOS image derived variables used in the current study provided higher accuracy, with R^2=0.41 for both LR and RF, and R^2=0.36 for XGBoost. CNN further outperformed all three, reaching an R^2 of 0.45. Among the evaluated approaches, the CNN model achieved the highest predictive performance, with an R^2 of 0.45. Previous studies on pine forests showed that there were different parameters (forest type, remote sensing data, sample size, method, etc.) playing a role in the AGB predictions. Including spectral vegetation indices derived from optical images has the potential to improve AGB estimation [39, 56]. Meanwhile, texture information of an optical image was reported as another positive feature that played a leading role in the improvement of forest AGB estimation studies by Günlü et al. [35]. Land surface temperature and soil moisture derived from Landsat data have a significant contribution to achieving lower RMSE of AGB prediction [66].

One of the limitations of this study is the small number of sampling sites. Li et al. [67] explored various modeling approaches to improve the accuracy of AGB estimations. Their study investigated the contribution of integrating remote sensing datasets with modeling approaches under conditions of limited data availability. Recent investigations have similarly noted that limited field measurements call for more complicated modeling strategies to maintain acceptable AGB estimation accuracy. These considerations further highlight the value of adopting advanced analytical frameworks when working with restricted ground-truth data. A substantial body of research has explored AGB estimation through varied combinations of field measurements and remote-sensing inputs. Among studies with a similarly constrained number of sample plots, Qazi et al. [68] worked with 51 plots across Nepal using ALOS-1 and GeoEye-1 imagery for biomass mapping. They found that, for AGB estimation using LR models, the validation R^2 was 0.44 for SAR imagery alone, whereas the results were significantly better with optical imagery (R^2 = 0.76). Similarly, Tavasoli and Arefi [69] used thiry nine circular sampling sites to estimate AGB. They applied the Genetic-Random Forest (GA-RF) machine learning algorithm with ALOS-1, Sentinel-1, and Sentinel-2 satellite imagery. Their combined ALOS and Sentinel-1 dataset achieved an R^2 of 0.72, whereas Sentinel-2 data used alone resulted in an R^2 of 0.62. Ji et al. [70] addressed AGB estimation across 61 sample sites by evaluating 15 different multi-band SAR configurations spanning X-, C-, L-, and P-band frequencies, and comparing MLSR, RF, and deep learning approaches.The top-performing configuration was an MLSR model that merged L- and P-band observations, reaching R^2=0.67 and RMSE=14.51 Mg ha^{-1}.

Overfitting risk and other difficulties tied to small training sets, along with mitigation strategies such as adding supplementary biophysical predictors, are recurring themes in the literature [71]. Li et al. [72] demonstrated that environmental variables, particularly soil properties, play an important role in forest biomass modeling. Their results indicated that soil and vegetation types jointly contribute significantly to AGB prediction accuracy, suggesting that incorporating soil-related information can substantially improve remote sensing–based biomass estimates. Kariofillia et al. [73] similarly studied carbon stock estimation in Mediterranean agricultural systems. They found that combining remote sensing layers with soil data substantially raised model performance, indirectly corroborating the added value of soil inputs for AGB prediction. The findings indirectly support the contribution of soil data to AGB prediction. In exploring the applicability of models for small datasets, a model developed by Zhou et al. [74] introduced as suitable for such data. This model has shown superior performance compared to others, especially in complex classification tasks and when working with a limited number of examples. Another limitation of this study is the lack of an extensive archive of remote sensing data, particularly optical data, to combine with SAR images. Additionally, there was no concurrent remote sensing data available at the time of fieldwork. However, as AGB generally exhibits limited temporal variability, the most recent and publicly accessible mosaic ALOS PALSAR data was utilized. Another limitation is the relatively small amount of ground-based AGB data. Increasing the volume of ground data could improve the accuracy of AGB estimation for pine forests, especially with the deployment of new C-band and L-band satellite missions. Textural data can be applied as an additional variable that contributed to the AGB estimation in both optical [36] and SAR images [65, 75]. A combination of multi-source remote sensing data can be also useful. Yavaşlı [76] showed the ability of combined Landsat and ICESat/GLAS laser altimeter to achieve better AGB estimation. Another factor for limitation could be the characteristics of the topography. As the samples were collected from different locations, the slope and aspect information may be added to improve the predictions. To address the negative impacts of topography on SAR imagery, various techniques and auxiliary data can be utilized during the image processing and evaluation stages [77, 78]. Radiometric terrain correction reduces terrain-induced backscatter variations by normalizing pixel values, while speckle filtering and multilook processing minimize noise and improve image quality. Geometric correction using high-resolution DEMs further reduces spatial distortions. Together, these preprocessing steps enhance the reliability of SAR data for biomass estimation and related analyses.

CONCLUSION

Black pine is among the dominant forest tree species in Türkiye and plays an important role in carbon sequestration and ecosystem resilience under changing climatic conditions. In this study, a 1D-CNN-based framework was developed for AGB estimation and compared with a conventional LR model. To evaluate the contribution of different input variables, twelve scenarios were generated using dual-polarized ALOS-PALSAR data. The results indicate that the CNN approach provides strong predictive capability for AGB estimation, while indices derived from dual-polarimetric SAR data considerably improve model performance. Moreover, the use of full-polarimetric SAR data may yield more informative feature sets, potentially increasing estimation accuracy and reducing RMSE.

Although the relatively limited sample size represents a constraint for both machine learning and deep learning applications, the CNN models demonstrated superior performance compared with conventional approaches. This performance may be related to the ability of CNN architectures to model complex, non-linear relationships, even when the number of input features is limited. Integrating these modeling approaches into national forest inventory and monitoring systems could improve biomass estimates and provide more reliable information on forest carbon stocks. Such information may support conservation planning, carbon accounting, and the development of sustainable forest management strategies in Türkiye and other forested regions. The use of data-driven methods in policy and management processes could also strengthen climate change mitigation efforts by improving the monitoring of biomass and carbon dynamics. Future studies could evaluate the effects of including additional explanatory variables and larger datasets, and integrating field-based measurements with remotely sensed and model-derived data to improve analytical robustness and model performance. Moreover, further studies may benefit from the combined use of multi-temporal and multi-frequency SAR datasets, along with multispectral optical imagery, to enhance biomass estimation accuracy and spatiotemporal analysis capabilities. A spatial AGB change detection analysis could be considered with further fieldwork studies. Archived ALOS-1 images and the forest inventory data provided beneficial results in understanding the AGB distribution for the Pinus nigra forest. Next-generation L-band missions (ALOS-4, NISAR, ROSE-L, and Tandem-L) can contribute to a spatio-temporal analysis to obtain biomass and carbon dynamics.

AUTHORSHIP CONTRIBUTIONS

Authors equally contributed to this work.

DATA AVAILABILITY STATEMENT

The ALOS-1 PALSAR mosaic is openly available on the website https://www.eorc.jaxa.jp/ALOS/en/dataset/fnf_e.htm

CONFLICT OF INTEREST

The author declared no potential conflicts of interest with respect to the research, authorship, and/or publication of this article.

FUNDING

This study was conducted as part of the project titled "Determination of carbon stocks in black pine (*Pinus nigra* Arn. subsp. *pallasiana*) plantations (ESK-10(6303)/2011-2014)" that was funded by the Turkish General Directorate of Forestry.

ETHICS

There are no ethical issues with the publication of this manuscript.

STATEMENT ON THE USE OF ARTIFICIAL INTELLIGENCE

Artificial intelligence was not used in the preparation of the article.

REFERENCES

[1] Lackner M, Sajjadi B, Chen Y. Introduction to climate change mitigation and adaptation. In: Lackner M, Sajjadi B, Chen WY, editors. Handbook of climate change mitigation and adaptation. 3rd ed. Switzerland: Springer; 2022. p. 3-21. [CrossRef]

[2] Leley NC, Langat DK, Kisiwa AK, Maina GM, Muga MO. Total carbon stock and potential carbon sequestration economic value of Mukogodo forest-landscape ecosystem in drylands of Northern Kenya. Open J For 2022;12:19-40. [CrossRef]

[3] Lorenz K, Lal R. Carbon sequestration in forest ecosystems. Springer; 2010. 277 p. [CrossRef]
[4] Shahabedini S, Ghahramany L, Pulido F, et al. Estimating leaf biomass of pollarded Lebanon oak in open silvopastoral systems using allometric equations. Trees (Berl) 2018;32:99-108. [CrossRef]
[5] Ameztegui A, Rodrigues M, Granda V. Uncertainty of biomass stocks in Spanish forests: A comprehensive comparison of allometric equations. Eur J For Res 2022;141:395-407. [CrossRef]
[6] Arseniou G, MacFarlane DW, Calders K, et al. Accuracy differences in aboveground woody biomass estimation with terrestrial laser scanning for trees in urban and rural forests and different leaf conditions. Trees (Berl) 2023;37:761-779. [CrossRef]
[7] Fleming AL, Wang G, McRoberts RE. Comparison of methods toward multi-scale forest carbon mapping and spatial uncertainty analysis: Combining national forest inventory plot data and Landsat TM images. Eur J For Res 2015;134:125-137. [CrossRef]
[8] Lu D, Chen Q, Wang G, Liu L, Li G, Moran E. A survey of remote sensing-based aboveground biomass estimation methods in forest ecosystems. Int J Digit Earth 2016;9:63-105. [CrossRef]
[9] Racine EB, Coops NC, Bégin J, Myllymäki M. Tree species, crown cover, and age as determinants of the vertical distribution of airborne LiDAR returns. Trees (Berl) 2021;35:1845-1861. [CrossRef]
[10] Coops NC, Tompalski P, Goodbody TRH, Achim A, Mulverhill C. Framework for near real-time forest inventory using multi-source remote sensing data. Forestry (Oxf) 2022. [CrossRef]
[11] Foody GM, Boyd DS, Cutler MEJ. Predictive relations of tropical forest biomass from Landsat TM data and their transferability between regions. Remote Sens Environ 2003;85:463-474. [CrossRef]
[12] Ghasemi N, Sahebi MH, Mohammadzadeh A. A review on biomass estimation methods using synthetic aperture radar data. Int J Geomat Geosci 2011;1:776-788.
[13] Ningthoujam RK, Joshi PK, Roy PS. Retrieval of forest biomass for tropical deciduous mixed forest using ALOS PALSAR mosaic imagery and field plot data. Int J Appl Earth Obs Geoinf 2018;69:206-216. [CrossRef]
[14] Englhart S, Keuck V, Siegert F. Aboveground biomass retrieval in tropical forests: The potential of combined X- and L-band SAR data use. Remote Sens Environ 2011;115:1260-1271. [CrossRef]
[15] George-Chacón SP, Milodowski DT, Dupuy JM, Mas JF, Williams M, Castillo-Santiago MA, et al. Using satellite estimates of aboveground biomass to assess carbon stocks in a mixed-management, semi-deciduous tropical forest in the Yucatan Peninsula. Geocarto Int 2021. [CrossRef]
[16] Li C, Li Y, Li M. Improving forest aboveground biomass (AGB) estimation by incorporating crown density and using Landsat 8 OLI images of a subtropical forest in western Hunan in Central China. Forests (Basel) 2019;10:104. [CrossRef]
[17] Shah SAA, Manzoor MA, Bais A. Canopy height estimation at Landsat resolution using convolutional neural networks. Mach Learn Knowl Extr 2020;2:23-36. [CrossRef]
[18] Zhang F, Tian X, Zhang H, Jiang M. Estimation of aboveground carbon density of forests using deep learning and multisource remote sensing. Remote Sens (Basel) 2022;14:3022. [CrossRef]
[19] Dong L, Du H, Han N, Li X, Zhu D, Ma F, et al. Application of convolutional neural network on Lei bamboo above-ground-biomass (AGB) estimation using WorldView-2. Remote Sens (Basel) 2020;12:958. [CrossRef]
[20] Cao R, Zhu J, Tu W, Li Q, Cao J, Liu B, et al. Integrating aerial and street view images for urban land use classification. Remote Sens (Basel) 2018;10:1553. [CrossRef]
[21] Ferreira MP, Lotte RG, D'Elia FV, Stamatopoulos C, Kim DH, Benjamin AR. Accurate mapping of Brazil nut trees (Bertholletia excelsa) in Amazonian forests using WorldView-3 satellite images and convolutional neural networks. Ecol Inform 2021;63:101302. [CrossRef]
[22] Bai T, Wang L, Yin D, Sun K, Chen Y, Li W, et al. Deep learning for change detection in remote sensing: A review. Geo-spat Inf Sci 2022. [CrossRef]
[23] Narin OG, Vatandaşlar C, Abdikan S. Estimating stand top height using freely distributed ICESat-2 LiDAR data: A case study from multi-species forests in Artvin. Forestist 2022;72:294-298. [CrossRef]
[24] Vidaković M. Conifers morphology and variation. Zagreb: Grafički zavod Hrvatske; 1991.
[25] Tutin TG, Akeroyd JR. Ranunculus L. In: Tutin TG, Burges NA, Chater AO, Edmondson JR, . Heywood VH, Moore DM, et al., editors. Flora Europaea. 2nd ed. Cambridge: Cambridge University Press; 1993. Vol. 1, p. 269-285.
[26] Güner A, Aslan S, Ekim T, Vural M, Babaç MT. Türkiye bitkileri listesi (damarlı bitkiler). İstanbul: Nezahat Gökyiğit Botanik Bahçesi ve Flora Araştırmaları Derneği Yayını; 2012. [Turkish]
[27] Davis PH. Flora of Turkey and the East Aegean Islands. Vol. 1. Edinburgh: Edinburgh University Press; 1965.
[28] Anşin R, Özkan ZC. Tohumlu bitkiler. Trabzon: Karadeniz Teknik Üniversitesi Orman Fakültesi Yayınları; 1993. Yayın No: 167/19.
[29] Kandemir A, Mataracı T. Pinus L. In: Güner A, Kandemir A, Menemen Y, Yıldırım H, Aslan S, Ekşi G, et al., editors. Resimli Türkiye Florası. Vol. 2. İstanbul: ANG Vakfı Nezahat Gökyiğit Botanik Bahçesi Yayınları; 2018. p. 324-354.

[30] GDF. Türkiye orman varlığı 2020. Ankara: T.C. Tarım ve Orman Bakanlığı, Orman Genel Müdürlüğü, Orman İdaresi ve Planlama Dairesi Başkanlığı; 2021. 56 p. [Turkish]
[31] Saatçioğlu F. Silvikültür I: Silvikültürün biyolojik esasları ve prensipleri. İstanbul: İstanbul Üniversitesi Orman Fakültesi Yayınları; 1969. 323 p. [Turkish]
[32] Durkaya A, Durkaya B, Cakil E. Predicting the above-ground biomass of Crimean pine (Pinus nigra) stands in Turkey. J Environ Biol 2010;31:115-118.
[33] Güner ST, Çömez A. Biomass equations and changes in carbon stock in afforested black pine (Pinus nigra Arnold. subsp. pallasiana (Lamb.) Holmboe) stands in Turkey. Fresenius Environ Bull 2017;26:2368-2379.
[34] Balenović I, Jazbec A, Marjanović H, Paladinić E, Vuletić D. Modeling tree characteristics of individual black pine (Pinus nigra Arn.) trees for use in remote sensing-based inventory. Forests (Basel) 2015;6:492-509. [CrossRef]
[35] Günlü A, Ercanlı I, Şenyurt M, Keleş S. Estimation of some stand parameters from textural features from WorldView-2 satellite image using the artificial neural network and multiple regression methods: A case study from Turkey. Geocarto Int 2021;36:918-935. [CrossRef]
[36] Turgut R, Günlü A. Estimating aboveground biomass using Landsat 8 OLI satellite image in pure Crimean pine (Pinus nigra J.F. Arnold subsp. pallasiana (Lamb.) Holmboe) stands: A case from Turkey. Geocarto Int 2022:1-15.
[37] Bulut S, Sivrikaya F, Günlü A. Evaluating statistical and combine method to predict stand above-ground biomass using remotely sensed data. Arab J Geosci 2022;15:838. [CrossRef]
[38] Vatandaşlar C, Abdikan S. Carbon stock estimation by dual-polarized synthetic aperture radar (SAR) and forest inventory data in a Mediterranean forest landscape. J For Res (Harbin) 2022;33:827-838. [CrossRef]
[39] Bulut S. Machine learning prediction of above-ground biomass in pure Calabrian pine (Pinus brutia Ten.) stands of the Mediterranean region, Türkiye. Ecol Inform 2023;74:10195. [CrossRef]
[40] Li Y, Li M, Li C, Liu Z. Forest aboveground biomass estimation using Landsat 8 and Sentinel-1A data with machine learning algorithms. Sci Rep 2020;10:9952. [CrossRef]
[41] Galdaki G, Zianis D, Gitas I, Radoglou K, Karathanassi V, Tsakiri-Strati M, et al. Vegetation biomass estimation with remote sensing: Focus on forest and other wooded land over the Mediterranean ecosystem. Int J Remote Sens 2017;38:1940-1966. [CrossRef]
[42] GDMRE. 1:500,000 scale geological inventory map series of Turkey. 2022 [cited 2022 Jan 17].
[43] IUSS Working Group WRB. World reference base for soil resources 2014, update 2015: International soil classification system for naming soils and creating legends for soil maps. World Soil Resources Reports No. 106. Rome: FAO; 2015. 192 p.
[44] GDM. Meteorological data. 2022. Available AT: https://mgm.gov.tr/ Accessed on Jan 17, 2022.
[45] Erinç S. Yağış müessiriyeti üzerine bir deneme ve yeni bir indis. İstanbul: Istanbul University Institute of Geography Press; 1965. [Turkish]
[46] Güner ŞT, Çömez A. Karaçam (Pinus nigra Arn. subsp. pallasiana) ağaçlandırma alanlarında karbon stoklarının belirlenmesi. Eskişehir: Orman Genel Müdürlüğü, Orman Toprak ve Ekoloji Araştırmaları Enstitüsü Müdürlüğü; 2014. Proje Sonuç Raporu: ESK-10(6303). 46 p. [Turkish]
[47] Shimada M, Itoh T, Motohka T, Watanabe M, Shiraishi T, Thapa R, et al. New global forest/non-forest maps from ALOS PALSAR data (2007-2010). Remote Sens Environ 2014;155. [CrossRef]
[48] Rodríguez-Veiga P, Quegan S, Carreiras J, Persson HJ, Fransson JE, Hoscilo A, et al. Forest biomass retrieval approaches from earth observation in different biomes. Int J Appl Earth Obs Geoinf 2019;77:53-68. [CrossRef]
[49] Vafaei S, Soosani J, Adeli K, Fadaei H, Naghavi H, Pham TD, et al. Improving accuracy estimation of forest aboveground biomass based on incorporation of ALOS-2 PALSAR-2 and Sentinel-2A imagery and machine learning: A case study of the Hyrcanian forest area (Iran). Remote Sens (Basel) 2018;10:172. [CrossRef]
[50] Yıldız S, Amasyalı MF. Iterative ensemble pseudo-labeling for convolutional neural networks. Sigma J Eng Nat Sci 2024;42:862-874. [CrossRef]
[51] Chen T, Guestrin C. XGBoost: A scalable tree boosting system. In: Proceedings of the 22nd ACM SIGKDD International Conference on Knowledge Discovery and Data Mining. 2016. p. 785-794. [CrossRef]
[52] Chen T, He T, Benesty M, Khotilovich V, Tang Y. xgboost: Extreme gradient boosting . 2018. Available at: https://cran.r-project.org/package=xgboost Accessed on Sep 14, 2026.
[53] Carmona P, Climent F, Momparler A. Predicting failure in the US banking sector: An extreme gradient boosting approach. Int Rev Econ Finance 2019;61:304-323. [CrossRef]
[54] Breiman L. Random forests. Mach Learn 2001;45:5-32. [CrossRef]
[55] Liaw A, Wiener M. randomForest: Breiman and Cutler's random forests for classification and regression. 2018. Available from: https://cran.r-project.org/package=randomForest Accessed on Sep 14, 2026.
[56] Günlü A, Ercanlı I, Başkent EZ, Çakır G. Estimating aboveground biomass using Landsat TM imagery: A case study of Anatolian Crimean pine forests in Turkey. Ann For Res 2014;57:289-298. [CrossRef]

[57] Huang JC, Tsai YC, Wu PY, Lien YH, Chien CY, Kuo CF, et al. Predictive modeling of blood pressure during hemodialysis: A comparison of linear model, random forest, support vector regression, XGBoost, LASSO regression and ensemble method. Comput Methods Programs Biomed 2020;195:105536. [CrossRef]

[58] Smith PF, Ganesh S, Liu P. A comparison of random forest regression and multiple linear regression for prediction in neuroscience. J Neurosci Methods 2013;220:85-91. [CrossRef]

[59] Schäfer J, Winiwarter L, Weiser H, Höfle B, Schmidtlein S, Novotný J, et al. CNN-based transfer learning for forest aboveground biomass prediction from ALS point cloud tomography. Eur J Remote Sens 2024;57. [CrossRef]

[60] Cartus O, Santoro M, Kellndorfer J. Mapping forest aboveground biomass in the Northeastern United States with ALOS PALSAR dual-polarization L-band. Remote Sens Environ 2012;124:466-478. [CrossRef]

[61] Basuki TM, Skidmore AK, Hussin YA, Van Duren I. Estimating tropical forest biomass more accurately by integrating ALOS PALSAR and Landsat-7 ETM+ data. Int J Remote Sens 2013;34:4871-4888. [CrossRef]

[62] Robinson C, Saatchi S, Neumann M, Gillespie T. Impacts of spatial variability on aboveground biomass estimation from L-band radar in a temperate forest. Remote Sens (Basel) 2013;5:1001-1023. [CrossRef]

[63] Fararoda R, Suraj Reddy R, Rajashekar G, Kiran Chand TR, Jha CS, Dadhwal VK. Improving forest above ground biomass estimates over Indian forests using multi-source data sets with machine learning algorithm. Ecol Inform 2021;65:101392. [CrossRef]

[64] Carreiras JMB, Melo JB, Vasconcelos MJ. Estimating the above-ground biomass in Miombo savanna woodlands (Mozambique, East Africa) using L-band synthetic aperture radar data. Remote Sens (Basel) 2013;5:1524-1548. [CrossRef]

[65] Günlü A, Ercanlı I. Artificial neural network models by ALOS PALSAR data for aboveground stand carbon predictions of pure beech stands: A case study from northern of Turkey. Geocarto Int 2020;35:17-28. [CrossRef]

[66] Jiang F, Kutia M, Ma K, Chen S, Long J, Sun H. Estimating the aboveground biomass of coniferous forest in Northeast China using spectral variables, land surface temperature and soil moisture. Sci Total Environ 2021;785:147335. [CrossRef]

[67] Li C, Li M, Iizuka K, Liu J, Chen K, Li Y. Effects of forest canopy structure on forest aboveground biomass estimation using Landsat imagery. IEEE Access 2021;9:5285-5295. [CrossRef]

[68] Qazi WA, Baig S, Gilani H, Waqar MM, Dhakal A, Ammar A. Comparison of forest aboveground biomass estimates from passive and active remote sensing sensors over Kayar Khola watershed, Chitwan district, Nepal. J Appl Remote Sens 2017;11:026038. [CrossRef]

[69] Tavasoli N, Arefi H. Comparison of capability of SAR and optical data in mapping forest above ground biomass based on machine learning. IECG 2020;13. [CrossRef]

[70] Ji Y, Wang L, Zhang W, Marino A, Wang M, Ma J, et al. Forest above-ground biomass estimation using X, C, L, and P band SAR polarimetric observations and different inversion models. Int J Digit Earth 2024;17:2310730. [CrossRef]

[71] Qiao J, Chen Z, Yu J, Cai R, Hao Z. Identification of causal structure in the presence of missing data with additive noise model. Proc AAAI Conf Artif Intell 2024;38:20516-20523. [CrossRef]

[72] Li Y, Li M, Liu Z, Li C. Combining Kriging interpolation to improve the accuracy of forest aboveground biomass estimation using remote sensing data. IEEE Access 2020;8:128124-128139. [CrossRef]

[73] Kariofillia P, Mimis A, Bithas K. Estimating biomass carbon stocks in agriculture land for the Mediterranean using remote sensing data. 2022. Available at: https://ageconsearch.umn.edu/record/337122?v=pdf Accessed on Sep 14, 2026.

[74] Zhou J, He Q, Cheng G, Lin Z. Union-net: Lightweight deep neural network model suitable for small data sets. J Supercomput 2023;79:7228-7243. [CrossRef]

[75] Thapa RB, Watanabe M, Motohka T, Shimada M. Potential of high-resolution ALOS PALSAR mosaic texture for aboveground forest carbon tracking in tropical region. Remote Sens Environ 2015;160:122-133. [CrossRef]

[76] Yavasli DD. Estimation of above ground forest biomass at Muğla using ICESat/GLAS and Landsat data. Remote Sens Appl Soc Environ 2016;4:211-218. [CrossRef]

[77] Flores-Anderson AI, Herndon KE, Thapa RB, Cherrington E. The SAR handbook: Comprehensive methodologies for forest monitoring and biomass estimation. 2019. Report No.: MSFC-E-DAA-TN67454.

[78] Guerra-Hernández J, Narine LL, Pascual A, Gonzalez-Ferreiro E, Botequim B, Malambo L, et al. Aboveground biomass mapping by integrating ICESat-2, SENTINEL-1, SENTINEL-2, ALOS2/PALSAR2, and topographic information in Mediterranean forests. GISci Remote Sens 2022;59:1509-1533. [CrossRef]

APPENDIX

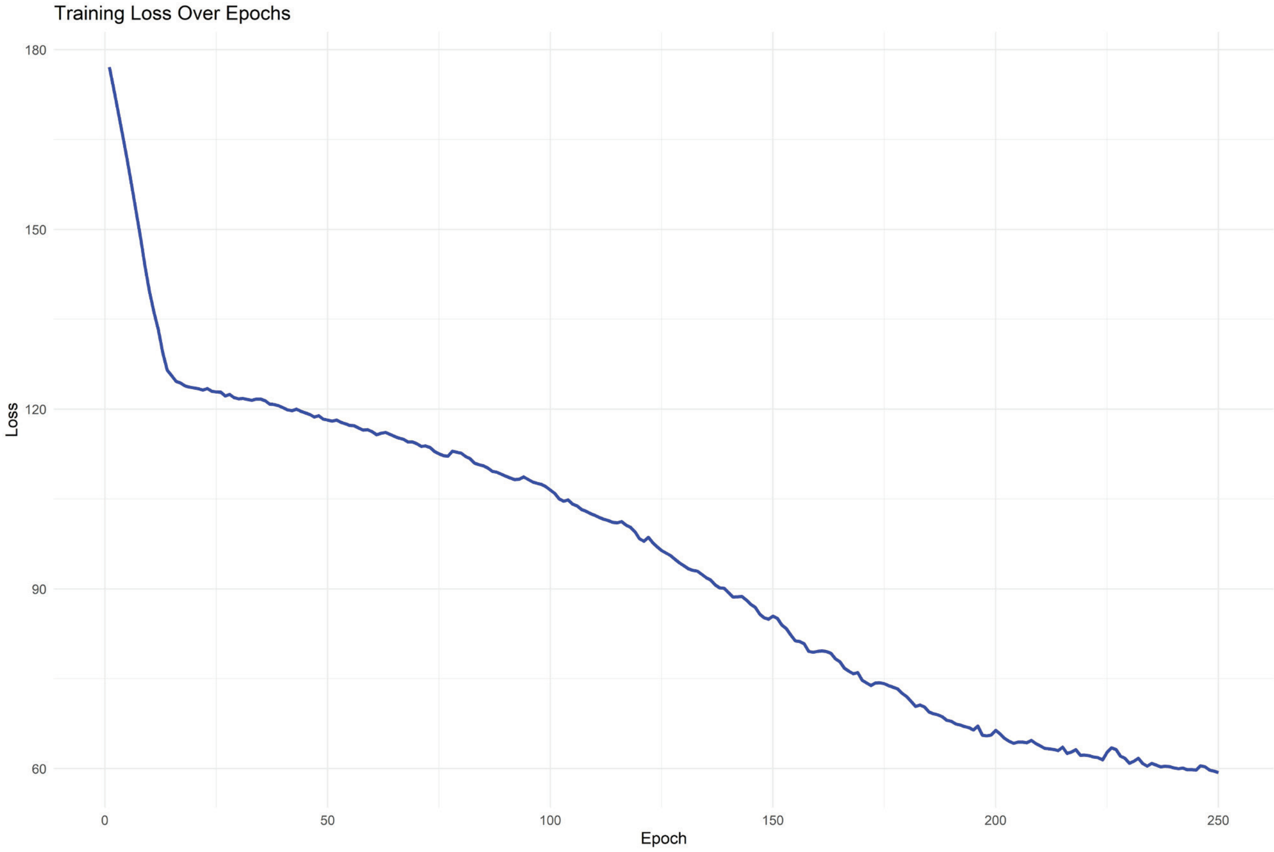

1. Test/loss graph of Scenario-9 for CNN method.

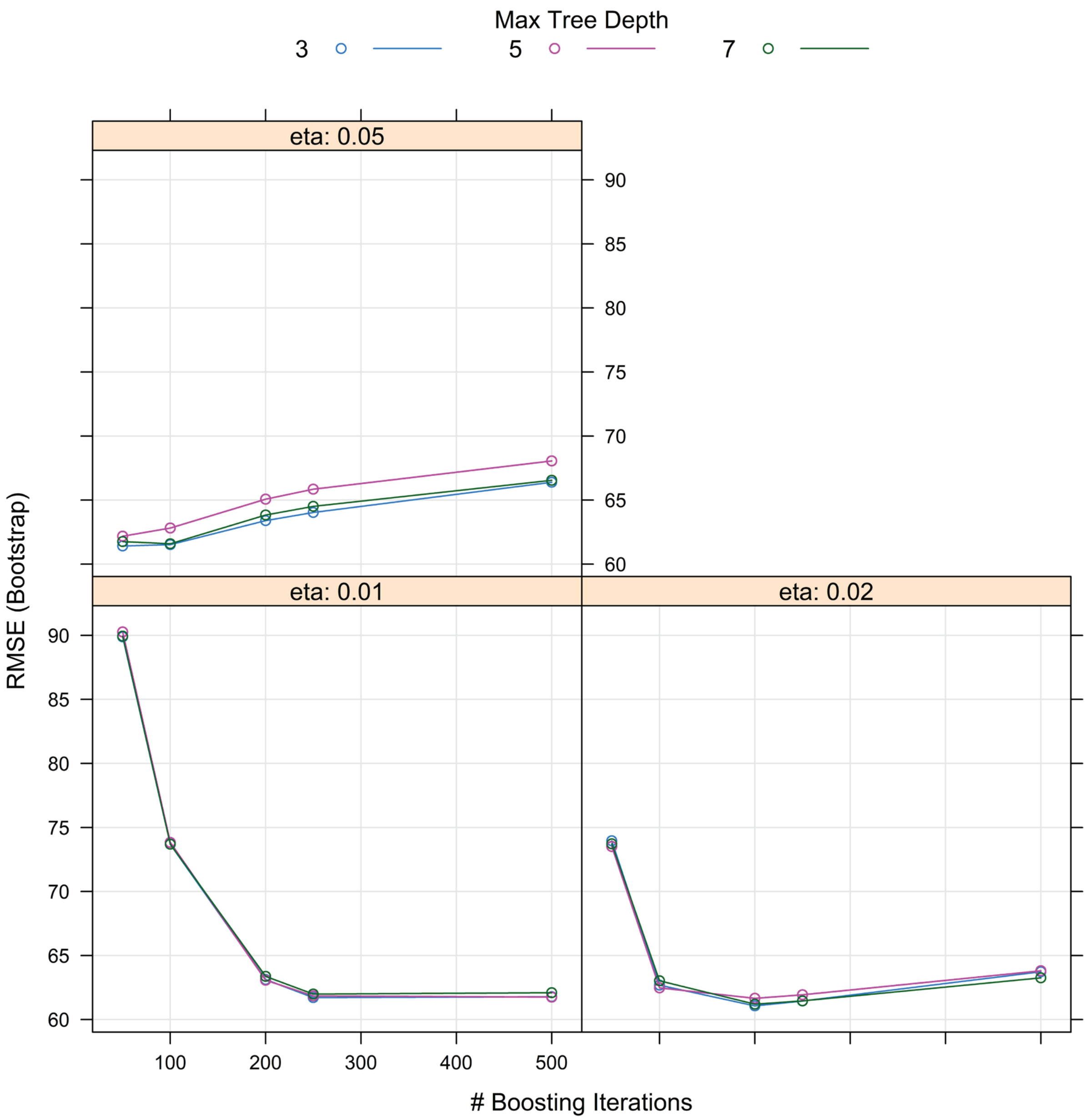

2. Grid search chart of ϒHH, ϒHV, ϒNDPI, ϒCPR variables for XGBoost.

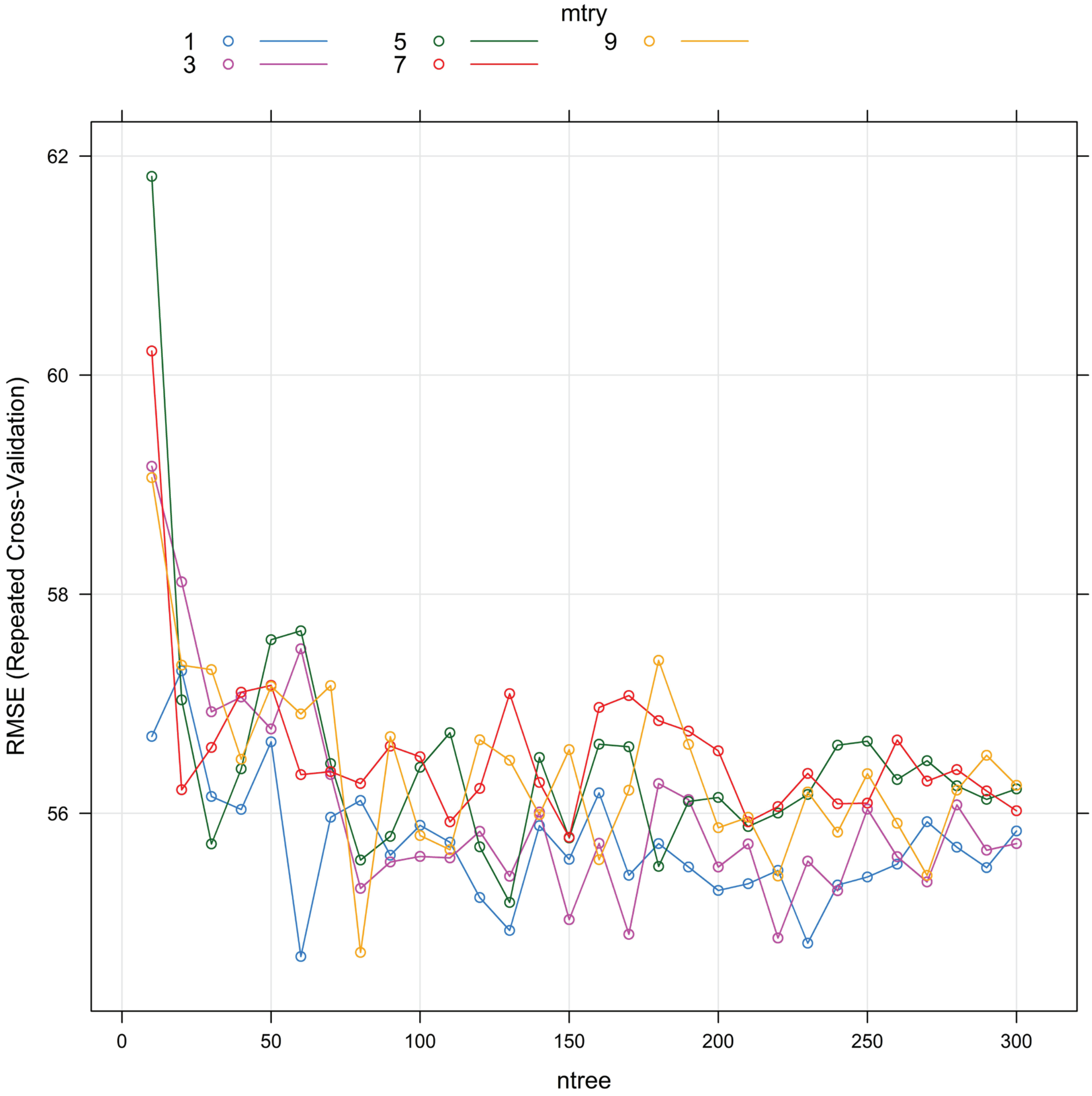

3. Grid search chart of ϒHH, ϒHV, ϒNDPI, ϒCPR variables for Random Forest.